Crystalline Structure in Thin Films of DEH−PPV Homopolymer and PPV-*b*-PI Rod−Coil Block Copolymers

Bradley D. Olsen,[†] Daniel Alcazar,[‡] Vahik Krikorian,[‡] Michael F. Toney,[§] Edwin L. Thomas,[‡] and Rachel A. Segalman*,[†]

Department of Chemical Engineering, University of California, Berkeley, Berkeley, California 94720, and Materials Science Division, Lawrence Berkeley Laboratory; Department of Materials Science and Engineering and Institute for Soldier Nanotechnologies, Massachusetts Institute of Technology, Cambridge, Massachusetts 02139; and Stanford Synchrotron Radiation Lab, Stanford Linear Accelerator Center, Menlo Park, California 94025

Received July 6, 2007; Revised Manuscript Received October 12, 2007

ABSTRACT: The rod orientation and crystalline packing of a model semiconducting rodlike polymer, poly-(2,5-di(2′-ethylhexyloxy)-1,4-phenylenevinylene) (DEH−PPV), is shown to affect the self-assembly of weakly segregated rod−coil block copolymers. The in-plane packing of DEH−PPV rods in lamellar poly(2,5-di(2′-ethylhexyloxy)-1,4-phenylenevinylene-*b*-isoprene) (DEH−PPV-*b*-PI) diblock copolymers is nearly identical to that observed in DEH−PPV homopolymers for compositions ranging from 0.42 to 0.82 vol % coil block. The crystal structure of DEH−PPV, characterized by grazing incidence X-ray diffraction and electron diffraction, consists of a tetragonal unit cell having $c = 0.665$ nm with $a = b = 1.348$ nm. The polymer chain axis is aligned along the [001] direction, and the nearest neighbor rod−rod spacing along ⟨110⟩ is 1.0 nm. As-cast thin films of DEH−PPV homopolymer demonstrate chain alignment primarily perpendicular to the substrate in 5100 g/mol homopolymer, while for 3500 g/mol homopolymer the chains align both perpendicular and parallel to the substrate. For the DEH−PPV-*b*-PI block copolymers, a sharper 001 reflection is observed due to the effect of microphase separation, improving alignment and stacking of the rods. The lamellar phases have a smectic A-like packing structure with the rods oriented parallel to the lamellar normal regardless of coil fraction; however, at coil fractions above about 0.8 the crystalline lattice of the rods becomes rapidly disordered as evidenced by loss of all but the two strongest Bragg reflections. This suggests that the constraints of packing into the unit cell outweigh the chain stretching and segment−segment repulsion energies that are predicted to lead to a transition from normal (smectic A) to tilted (smectic C) rod orientation within the lamellae at high coil fraction; increasing coil fraction breaks apart the crystalline lattice rather than distorting it into a tilted polymorph.

Introduction

Semiconducting polymers have attracted a great deal of interest for their promise to produce inexpensive and flexible LEDs, transistors, and photovoltaic cells.[1−3] The optimization of these devices requires control over the morphology of the active layer,[4,5] and both the chemical structure of the semiconducting polymers and the processing approaches used to fabricate devices have been varied in an attempt to kinetically induce desirable but nonequilibrium morphologies in many of these devices.[1−5] An alternative, especially in multicomponent devices, is to self-assemble a thermodynamically stable active layer using semiconducting block copolymers.[6−10] Block copolymers are an attractive option for their ability to form microphase structures on the 10 nm length scale[11] of exciton diffusion, and the equilibrium nature of block copolymer microphases promises more stable structures and longer device lifetimes. While much is known about nanopatterning with traditional block copolymers,[12] the incorporation of a rodlike semiconducting block into a block copolymer results in a rod−coil molecular structure and significant changes in the observed phase behavior compared to flexible, noncrystalline block copolymers.[13−17] The phase diagram for these materials has been mapped out in the weakly segregated limit using model poly-(alkoxyphenylenevinylene-*b*-isoprene) (PPV-*b*-PI) copolymers, demonstrating lamellar, nematic, and isotropic phases.[18,19]

The nanopatterning of rod−coil block copolymers for organic optoelectronics requires an understanding of their self-assembly in thin films where geometric confinement and surface segregation play a large role in determining the microphase structure. While the self-assembly of traditional block copolymers in thin films has been extensively studied,[12,20,21] relatively little is known about rod−coil block copolymer thin films. Often, the solution casting processes used to prepare rod−coil block copolymer films result in the deposition of kinetically trapped aggregates,[22−27] liquid crystalline defect patterns,[28−30] or phase-separated morphologies.[31] While these solution self-assembly techniques enable one to access a wide variety of interesting morphologies, a strong dependence of the morphology on precise processing history provides a formidable barrier to the application of block copolymers.[32,33] In addition, the nonequilibrium nature of these morphologies makes them likely to evolve in a poorly controlled way during subsequent device processing steps. Microphase separation has also been achieved by thermal annealing of films,[34,35] and using the model poly(2,5-di(2′-ethylhexyloxy)-1,4-phenylenevinylene-*b*-isoprene) (DEH−PPV-*b*-PI) system in which thermally reversible phase transitions may be accessed, we have recently demonstrated the growth of well-ordered lamellar structures in thin films starting from a kinetically trapped as-cast isotropic state.[36] In thin films the lamellae are oriented primarily parallel to the substrate, while in thicker films the lamellae take a bimodal orientation both parallel and perpendicular to the substrate.

* Corresponding author: e-mail segalman@berkeley.edu.
[†] University of California, Berkeley.
[‡] Massachusetts Institute of Technology.
[§] Stanford Linear Accelerator Center.

10.1021/ma0714971 CCC: $40.75
Published on Web 12/08/2007

Table 1. Polymer Molecular Properties

polymer	PPV M_n (g/mol)	PPV PDI	PI M_n (g/mol)	PI PDI	N	ϕ_{coil}
DEH−PPV-3.5	3500	1.17			47	0
DEH−PPV-5.1	5100	1.07			68	0
DEH−PPVbPI-42	3500	1.17	2400	1.05	82	0.42
DEH−PPVbPI-67	3400	1.17	6300	1.03	138	0.67
DEH−PPVbPI-72	3500	1.17	8100	1.02	166	0.72
DEH−PPVbPI-82	3400	1.17	13900	1.02	249	0.82

One powerful opportunity in the self-assembly of rod−coil block copolymers is for simultaneous control of the structure on the dual length scales of block copolymer self-assembly (∼10 nm) and liquid crystalline rod−rod packing (∼1 nm). It has been theoretically predicted that a liquid crystalline transition from smectic A-like to smectic C-like lamellar structure can occur with changing coil fraction without large changes in the nature of the microphase-separated lamellar structure.[37−39] These changes in rod orientation may have a profound effect on the properties of the microphase-separated state; in semiconducting polymers carrier mobility and optical properties show a strong orientational dependence due to the anisotropy of the properties of the single polymer molecules.[40,41] However, direct measurement of the rod orientation relative to the microphase structure is difficult with polycrystalline samples,[14,16] and the liquid crystalline structure of the lamellar microphases[18,19] has not been determined.

Elucidation of the crystalline or liquid crystalline structure within rod−coil block copolymers requires clear knowledge of the crystalline structure of the rod block itself. In the case of our model system with experimentally accessible phase transitions, knowledge of the DEH−PPV crystal structure is critical to determine rod orientation within the lamellar microphase. Unsubstituted (insoluble) poly(phenylenevinylene) (PPV) packs into a monoclinic unit cell with herringbone packing of the PPV chains[42−45] and a repeat unit length in very close agreement with the theoretical value of 0.665 nm.[46,47] The crystal structure of PPV changes dramatically with the addition of short side chains,[48−50] and the polymer remains semicrystalline even with the addition of relatively large side groups.[51−54] The most widely studied functionalized PPVs, poly(2-methyloxy-5-ethylhexyloxyphenylenevinylene) (MEH−PPV) and poly(2,5-dioctyloxyphenylenevinylene) (DOO−PPV), form semicrystalline structures where each crystallite is composed of a layered or fibrilar structure of PPV chains[51,52] with the chain axes aligned parallel to the substrate in thin films.[55−57] Very limited structural data are available for the more soluble DEH−PPV used in our block copolymers.[34,54] DEH−PPV is also crystalline at room temperature, and it transitions through smectic, nematic, and isotropic phases on heating. The crystalline and smectic phases form layered structures where each layer is the width of a single molecule, and the chain axes are aligned normal to the layers in both the crystalline and smectic phases; however, the crystallographic lattice is not known.[54]

The present work presents a detailed characterization of the crystalline structure of DEH−PPV homopolymer and within weakly segregated lamellar DEH−PPV-*b*-PI block copolymer films in order to understand the liquid crystalline rod alignment within the microphase-separated structures. We determine the type of unit cell, its dimensions, and the Laue class of DEH−PPV. Comparing the homopolymer diffraction patterns to those of DEH−PPV-*b*-PI rod−coil block copolymers shows that the crystalline structure is not significantly altered in the block copolymers. The bimodal orientation of the microphase structure within thin films results in partially aligned samples, allowing the rod orientation relative to the microphase structure to be determined for the first time in rod−coil block copolymer thin films.

Experimental Methods

Poly(2,5-di(2′-ethylhexyloxy)-1,4-phenylenevinylene) (DEH−PPV) homopolymers and poly(2,5-di(2′-ethylhexyloxy)-1,4-phenylenevinylene-*b*-isoprene) (DEH−PPV-*b*-PI) block copolymers were synthesized as described previously.[18] Table 1 lists molecular weights and coil fractions for the materials studied. The number of repeat units, N, is calculated on the basis of a reference volume of one isoprene repeat unit. The polydispersity of the DEH−PPV blocks ranged between 1.07 and 1.17, and the polydispersities of all the PI blocks were less than 1.05. All of the block copolymers formed lamellar phases when thermally annealed and cooled from the isotropic phase in bulk and had thermally reversible order−disorder transitions, as determined by small-angle X-ray scattering (SAXS) and transmission electron microscopy (TEM). The complete phase diagram in this block copolymer system is published elsewhere.[18,19,58] The rod homopolymers are crystalline at room temperature and melt at 60 °C.[54]

Thin film samples for scanning force microscopy (SFM) and grazing-incidence X-ray diffraction (GIXD) were prepared by spin-casting polymers from toluene solution onto (100) silicon wafers with a native oxide surface (University Wafer, Boston, MA). Concentrations from 5 to 40 mg/mL and spin speeds between 900 and 6000 rpm were used to control the film thicknesses. Since toluene is a good solvent for both blocks and the polymer concentrations are low, spin-casting solutions are isotropic. The as-cast block copolymer films did not demonstrate liquid crystalline order or microphase separation due to trapping of the disordered solution state. Samples of PPVbPI-42, -67, and -72 (number denotes coil volume fraction) were annealed above the melting temperature of the rod at 80 °C under vacuum for 24 h, while samples of PPVbPI-82 were annealed under ambient conditions for 48 h because films dewet at elevated temperatures. Samples of DEH−PPV homopolymers were analyzed as-cast. Sample thicknesses were measured prior to thermal annealing using a Sentech SE400 ellipsometer with a 632.8 Å laser. Film thicknesses for the block copolymers have been nondimensionalized in terms of the bulk domain spacing of each polymer, and the symbol l is used to represent the thickness of a single lamellar domain spacing. SFM samples were imaged on a Digital Instruments MultiMode AFM operating in tapping mode.

GIXD experiments were performed at beamline 11-3 of the Stanford Synchrotron Radiation Lab using a previously described experimental geometry.[59] Experiments were performed using a 0.9736 Å X-ray beam with a width of 150 μm and a height of 50 μm. Data were recorded on a 2D MAR345 image plate detector (pixel size 0.15 mm) with a sample-to-detector distance of 433 mm. Data were acquired for 20 min per frame at an incident angle of 0.1° (above the critical angle for these films but below the critical angle for Si such that the X-rays penetrated throughout the depth of the polymer film but did not penetrate into the SiO_2/Si substrate). Scattering angles were converted into q-space accounting for the planarity of the detector. The q_z and q_{xy} axes were calculated using the direct beam as the reference beam. Linecuts were taken by averaging over a width of 21 pixels perpendicular to the direction of the cut. Scattering intensities were reported in arbitrary units, and all 2D images were plotted on a linear scale.

Single crystals of DEH−PPV homopolymer were prepared by dissolving a small amount of polymer in chloroform and adding

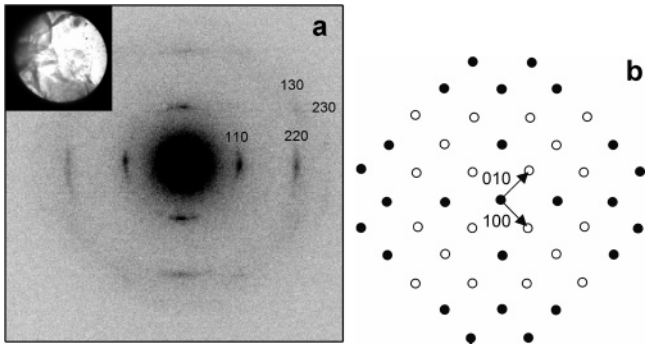

Figure 1. TEM electron diffraction from a single crystalline region of DEH−PPV homopolymer. (a) Single crystals of DEH−PPV-5.1 show diffraction patterns with 4-fold symmetry when imaged along the 001 zone axis. The 110 peak indicates a rod−rod spacing of 0.95 nm. The defocused diffraction image in the inset shows that the diffracting region is composed of several crystals; however, because of variations in the crystallographic orientation, only a small number of slightly rotated crystals satisfy the diffraction condition. (b) Schematic of the reciprocal lattice shows dark spots for observed peaks and light spots for absent peaks. In particular, all *h*00 and 0*k*0 reflections are absent.

methanol until the polymer became barely soluble. The solution was allowed to sit overnight to induce precipitation through the preferential evaporation of chloroform from the solution. Crystallites collected at the air/liquid interface due to the high density of the chloroform/methanol solution. Crystallites were then pipetted off the surface of the solution onto carbon-coated copper grids. Samples were not stained. Electron diffraction patterns were taken on a JEOL 2010F TEM equipped with a field-emission gun and a postcolumn Gatan imaging filter (GIF) operating at 200 keV. Polycrystalline diffraction patterns and bright field images were taken on a JEOL 2000FX with a LaB_6 filament operating at 200 keV. Both microscopes were operated in low dose/beam sensitive mode.

To aid in understanding how the polymer packs within its unit cell, the size of the DEH−PPV monomer unit was estimated using a MM2 molecular mechanics simulation in ChemSoft Chem3D Ultra. Energy minimization calculations were carried out on a DEH−PPV trimer, and estimates of the molecular size were made using the central repeat unit to most accurately reproduce the steric environment found in the polymer chain.

Results and Discussion

Crystal Structure of DEH−PPV Homopolymer. The crystalline structure of DEH−PPV homopolymer is partially determined using a combination of selected area electron diffraction (SAED) on small single crystals and GIXD of thin films. While electron diffraction allows diffraction patterns to be observed from single crystals and helps to identify the symmetry of the unit cell, GIXD reveals a larger number of reflections due to the increased stability of the polymer to X-rays that allows all three of the unit cell parameters to be quantified. Electron diffraction of small areas produces (*hk*0) single-crystal diffraction patterns that illustrate the symmetry of the DEH−PPV unit cell and show a significant number of higher-order peaks, as shown in Figure 1. We examined a large variety of crystallite orientations and found only 2-fold and 4-fold symmetric patterns. The electron diffraction pattern with 4-fold symmetry in Figure 1a has been indexed according to the smallest unit cell convention such that the 110 peak is the first peak and higher-order peaks correspond to the 220, 310, and 320 reflections. The location of the 320 peak is inconsistent with the indexing scheme where the primary peak corresponds to the 100 reflection. The diffraction pattern is identified as being taken along the 001 zone axis (along the chain axis of the PPV molecule) due to the fact that 4-fold symmetry is most likely

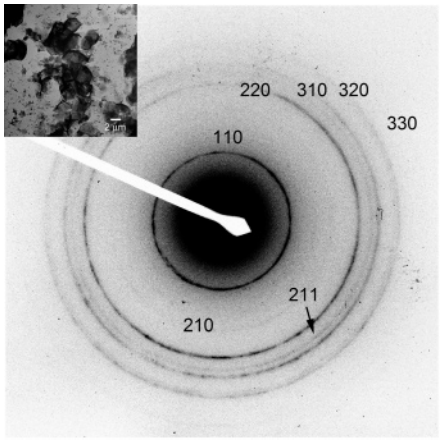

Figure 2. Electron diffraction of polycrystalline region of DEH−PPV homopolymer. Because of the increased scattering volume in a polycrystalline sample of PPV-5.1, a larger number of reflections are observed in the electron diffraction pattern of the polycrystalline sample than in that of the small single crystalline regions. The peak indexing matches that of the GIXD patterns, and the peak positions measured by the two techniques are in agreement to within a few percent. The bright field image (inset) shows aggregates of a large number of micron-sized single crystals.

Table 2. Peak Locations in DEH−PPV Homopolymer

	GIXD		ED	
peak	q/q^* (exp)	q/q^* (theory)	q/q^* (exp)	q/q^* (theory)
110	1.000	1.000	1.000	1.000
210	1.607	1.581	1.595	1.581
220	2.007	2.000	1.975	2.000
310	2.286	2.236	2.247	2.236
320	2.565	2.550	2.530	2.550
330	2.984	3.000	2.928	3.000
001	1.449	1.449		
101	1.579	1.612		
111	1.774	1.760		
211	2.179	2.143	2.143	2.143
301	2.619	2.567		

to arise between the equivalent in-plane packing directions of the layered crystal structure ([100] and [010] directions). Two-fold symmetric patterns show only 110 and 220 peaks. These crystallites are viewed along a [*hhl*] zone axis such that 110 reflections are observed but $1\bar{1}0$ reflections are not. Polycrystalline regions are also commonly observed due to the random tilt and overlap of the crystallites; the spots in these patterns may be accounted for by the superposition of a small number of 4- and 2-fold symmetric patterns from independently scattering crystallites.

Selected area electron diffraction (SAED) of a strongly scattering aggregate of DEH−PPV single crystals shows a series of higher-order peaks beyond those observed by SAED, as shown in Figure 2. The strong scattering that results in a larger number of high-order peaks is due to the increased scattering volume in the polycrystalline sample. The diffraction pattern shows four strong reflections corresponding to the 110, 220, 310, and 320 spots observed by electron diffraction from larger single crystals. In addition, three weaker reflections are observed corresponding to the 210, 211, and 330 peaks. We note that although crystallites of many orientations were examined, few peaks from first- or higher-order Laue zones are observed in the electron diffraction patterns. Table 2 shows theoretical and experimental ratios of the peak positions to the primary 110 peak, indicating agreement between the experimental ED pattern and the peak indexing scheme to within a few percent.

Combining GIXD data with the electron diffraction results allows all three unit cell parameters to be quantified. GIXD

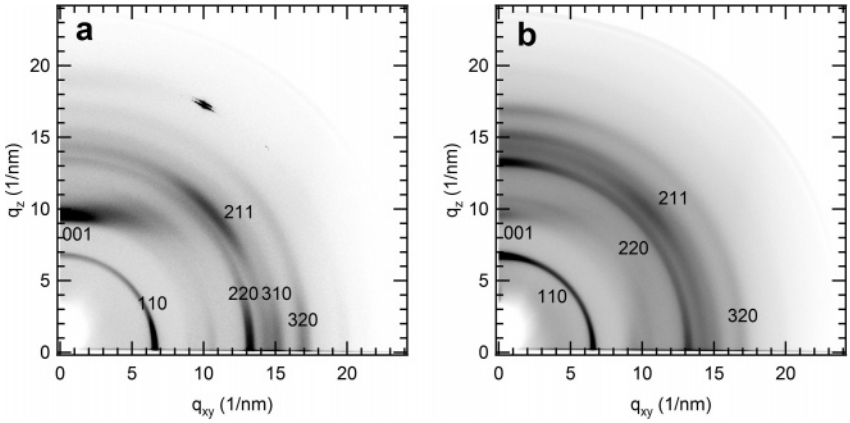

Figure 3. GIXD of DEH−PPV homopolymers: (a) DEH−PPV-5.1, film thickness 92 nm; (b) DEH−PPV-3.5, film thickness 94 nm. DEH−PPV shows crystalline structures when spun-cast into thin films. The peak/ring at about 6.6 1/nm is the 110 peak from the rod−rod packing in the plane of the smectic layers, and the peak at approximately 9.5 1/nm along the q_{xy} axis corresponds to the monomer unit length aligned along the 001 crystallographic direction. The angular distribution of intensities suggests that in the 5100 g/mol PPV the molecules are aligned primarily perpendicular to the film, while the 3500 g/mol PPV has a mixed distribution parallel and perpendicular to the film. The highest q peak in (a) is an experimental artifact due to silicon dust on the sample.

patterns, shown in Figure 3, demonstrate a large number of Bragg reflections representative of all three directions in reciprocal space. Refraction shifts of peak positions due to scattering in the distorted wave Born approximation are negligible for the angles at which reflections are observed in this study. In both DEH−PPV homopolymers investigated, an intense ring is clearly observable at 6.60 1/nm, corresponding to the 110 peak in the electron diffraction pattern. In the 5100 g/mol sample, the ring has greatest intensity near the $q_z = 0$ axis. An intense reflection is observed orthogonal to the 110 reflection (along the vertical cut) at 9.57 1/nm, as illustrated in Figure 4. The location of each cut from the 2D scattering pattern is illustrated in the insets. After adjustment for the refraction effects in the thin film using the DWBA, the peak along q_z from the vertical cut (close to specular) corresponds to a spacing of 0.665 nm. This spacing matches very closely with the 001 unit cell dimension measured for unsubstituted PPV.[42−45] Consistent with the fact that the length of a PPV monomer unit should not depend strongly on the side group and the fact that the reflection is observed orthogonal to the 110 plane, this peak is assigned as the 001 reflection in DEH−PPV.

Identification of the 110 and 001 reflections allows for complete indexing of the GIXD pattern, as shown in the linecuts in Figure 4. Figure 4a shows a linecut along the $q_z = 0.22$ 1/nm axis that corresponds to the q_z for specular reflection; this linecut primarily contains reflections from the zeroth-order Laue zone. Figure 4b shows a vertical linecut, showing the intense 001 reflection as well as several weaker reflections perpendicular to the film interface. Figure 4c shows a linecut along $q_z = 9.57$ 1/nm corresponding to the location of the 001 peak; this linecut illustrates a number of reflections in the first-order Laue zone. A comparison between the theoretical and experimental peak ratios between reflections in the zeroth- and first-order Laue zones and the 110 peak is shown in Table 2, indicating that the indexing scheme is consistent with that of the electron diffraction patterns and predicts the peak positions to within a few percent.

On the basis of the symmetry of these diffraction patterns, DEH−PPV packs into a tetragonal lattice with a lattice constant of 0.665 nm in the 001 direction and 1.348 nm in the 100 and 010 directions. Since the GIXD patterns are generated from samples that are polycrystalline in the plane of the film, it is not possible to differentiate between the two different Laue classes that correspond to a tetragonal unit cell, 4/*m* and 4/*mmm*. The 001 dimension of the unit cell very nearly matches the

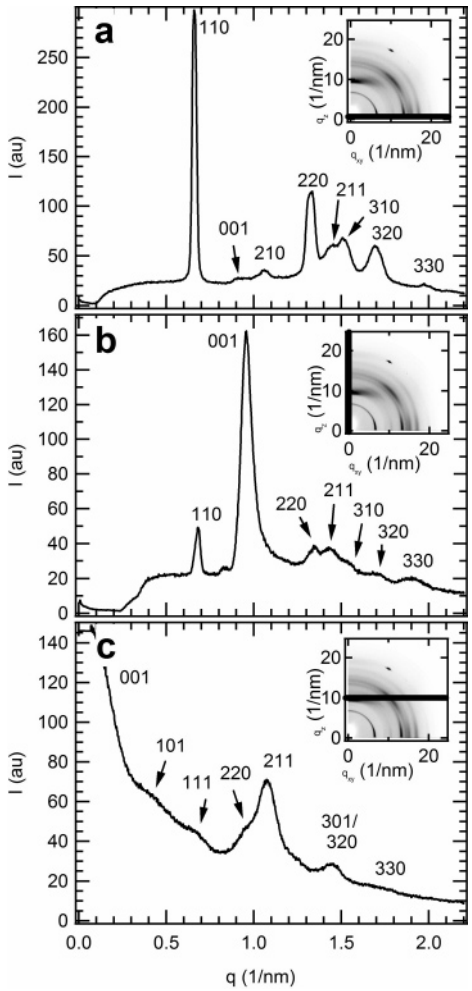

Figure 4. Linecuts through 2D GIXD patterns of DEH−PPV homopolymer (PPV-5.1, 92 nm thick): (a) horizontal linecut taken at $q_z = 0.22$ 1/nm, the q_z for specular reflection; (b) vertical cut; (c) horizontal cut taken at $q_z = 9.57$ 1/nm corresponding to the position of the 001 reflection. Bold lines in the insets show the positions of the linecut through the two-dimensional image. Peak indexing corresponds to a tetragonal lattice. Assuming a centered unit cell, the 110 peak corresponds to an in-plane packing distance of 0.97 nm, and the 001 peak corresponds to a chain repeat length of 0.665 nm. While peaks predominantly from the zeroth-order Laue zone are observed in the linecut at $q_z = 0.22$ 1/nm and primarily peaks from the first-order Laue zone are observed in the linecut at $q_z = 9.57$ 1/nm, the distribution of crystallite orientation causes some of the reflections to be observed in multiple linecuts.

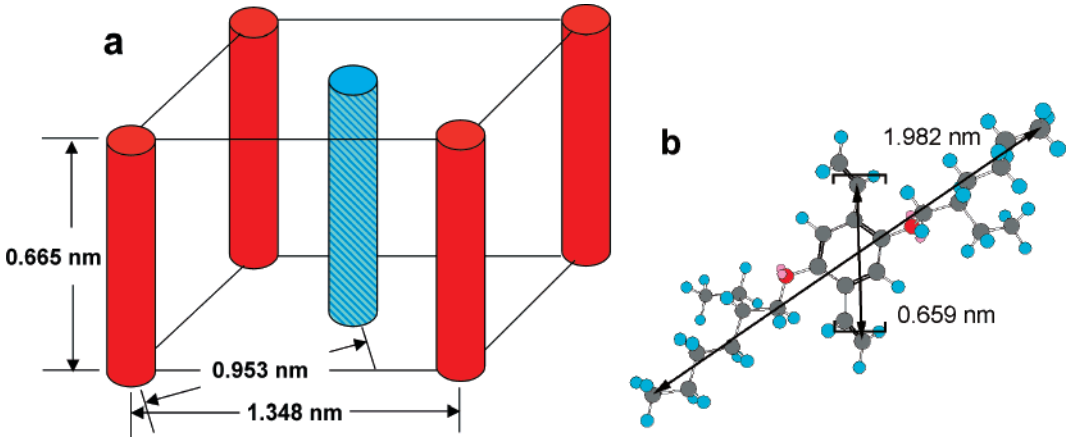

Figure 5. Schematic of the DEH−PPV unit cell and molecular dimensions. (a) DEH−PPV chains pack into a tetragonal unit cell with dimensions 1.348 nm in the [100] and [010] directions and 0.665 Å in the 001 direction. Chains are oriented parallel to the [001] direction, and the monomer length corresponds closely to the [001] unit cell dimension. Two chains pack into each unit cell. The absence of all *h*00 reflections indicates that this is a primitive unit cell, so the center chain is structurally unique from the corner chains. Potential differences between the center chain and corner chains include a translation along the [001] direction, opposite helical twist, and differences in side-chain conformation. (b) Structure of a DEH−PPV monomer unit in its energy-minimized conformation gives an approximate monomer length of 0.659 Å measured along the chain axis and a total end-to-end side-chain width of 1.982 nm with the side chains in an extended conformation. Although the side-chain conformation cannot be determined from the diffraction data, the fully extended length suggests that the chain dimensions are reasonable given the size of the unit cell. Brackets denote the DEH−PPV repeat unit.

length of a DEH−PPV monomer unit (0.659 nm calculated by quantum chemical energy minimization or 0.665 nm for unsubstituted PPV[42−45]), suggesting that the PPV molecules are oriented parallel to the 001 direction. The density of DEH−PPV thermally annealed into a semicrystalline state has been previously determined to be 0.99 g/cm^3 using a density column.[18] On the basis of a unit cell volume of 1.208 nm^3 and a monomer molecular weight of 347 g/mol, this corresponds very closely to two monomer units per unit cell and a unit cell density of 0.95 g/cm^3. The unit cell density may be lower than the total density due to dense packing of end groups outside the crystalline regions.

A number of systematic absences are observed in the diffraction pattern, most strikingly the absence of all *h*00 and 0*k*0 peaks in both the SAED and GIXD patterns. These absences imply the presence of additional symmetries within the unit cell. On the basis of the low-order diffraction peaks that are observed, the lattice may be identified as a P (primitive) type. This overall structure is illustrated schematically in Figure 5, showing two chains packed into a tetragonal lattice with the chain axes parallel to the 001 direction. The exact arrangement of the two chains within the unit cell cannot be experimentally determined. Instead, one of the chains has been arbitrarily centered along the edge of the unit cell and the second has been placed approximately equidistant from the four edges based on the single observed nearest-neighbor rod−rod spacing peak in the diffraction patterns. The fact that the diffraction peaks cannot be indexed according to a smaller unit cell indicates that the conformation of the central chain is distinct from that of the corner chains, though the details of this conformational contrast are unclear. The unique coloring of the central chain indicates that it distinct from the corner chains, to depict that the diffraction pattern is not consistent with a body-centered-cubic lattice.

The intensity of peaks in the first-order Laue zone is dependent upon the alignment of the DEH−PPV rods due to the effect of the film interface on the degree of crystalline order observed along the *c*-axis of the unit cell. Although the 001 reflection is very strong in the beamstop direction of the GIXD patterns for both DEH−PPV homopolymers and DEH−PPV-*b*-PI block copolymers, it is extremely weak or absent in all

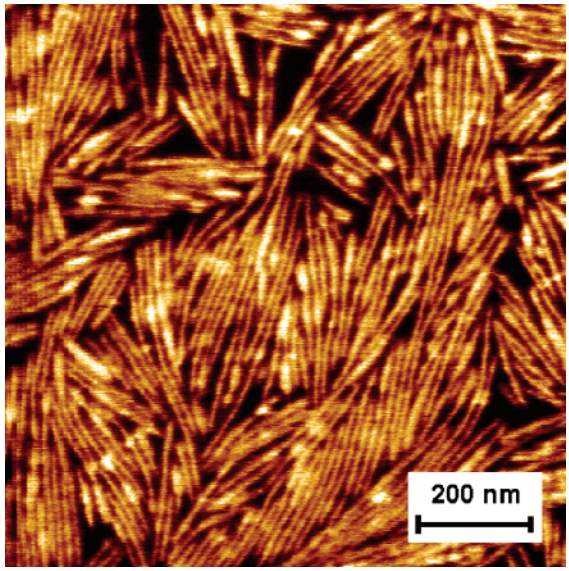

Figure 6. SFM image of a DEH−PPV*b*PI-42 block copolymer film. SFM phase images of the GIXD samples show surface structures of alternating light (PPV-rich) and dark (PI-rich) regions indicative of lamellar structures aligned perpendicular to the surface of the film. For the thicknesses studied the lamellar nanodomains at the vacuum interface are predominantly oriented perpendicular to the film surface while parallel oriented lamellae persist within the film. Rod orientation within these lamellar structures is determined by X-ray diffraction. The film thickness is 222 nm (16.0 lamellar layers).

single crystalline electron diffraction patterns, the polycrystalline electron diffraction pattern (Figure 2), and the equatorial direction of the GIXD patterns of homopolymers and block copolymers (Figures 4a and 8). In addition, previous studies of bulk DEH−PPV and DEH−PPV-*b*-PI showed extremely weak or absent 001 reflections around 9.55 1/nm.[18,54] The presence of only weak reflections from the first-order Laue zone in ED and bulk X-ray diffraction measurements indicates that the crystallites contain a large amount of axial disorder, similar to that observed in aromatic polyesters[60,61] and poly(β-propiolactone) crystals.[62] When the *c*-axis is oriented parallel to the interface normal, surface templating of the rod layers results in increased axial registration between rods and strong scattering

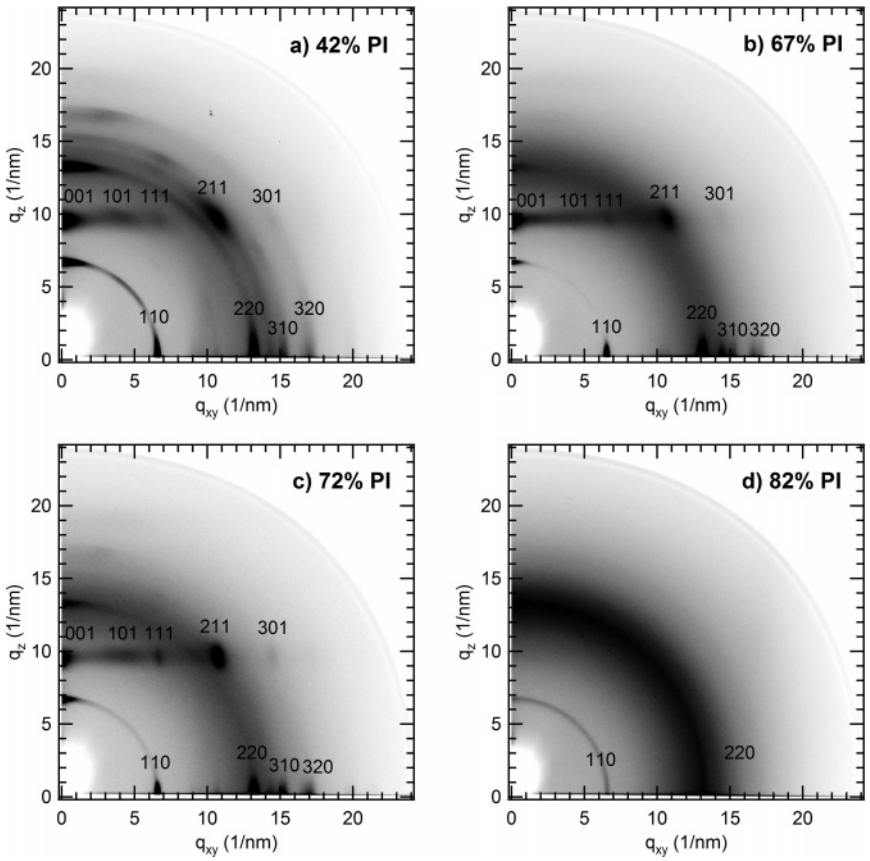

Figure 7. GIXD of PPV-*b*-PI block copolymers: (a) PPVbPI-42, film thickness 141 nm (10.2*l*); (b) PPVbPI-67, film thickness 212 nm (9.9*l*); (c) PPVbPI-72, film thickness 175 nm (7.1*l*); (d) PPVbPI-82, film thickness 154 nm (5.1*l*). The DEH−PPV rod crystalline structure in PPV-*b*-PI block copolymers is nearly identical to that observed in DEH−PPV homopolymers. Sharper peaks in the first Laue zone indicate an improvement in ordering along the 001 direction due to the effect of microphase separation on restricting rod translation. Increasing coil fraction results in a rapid disordering of the lattice between 72% and 82% PI. At the highest coil fraction studied, scattering from the DEH−PPV lattice is overwhelmed by the amorphous halo from the PI block that overlaps with the 220 peak.

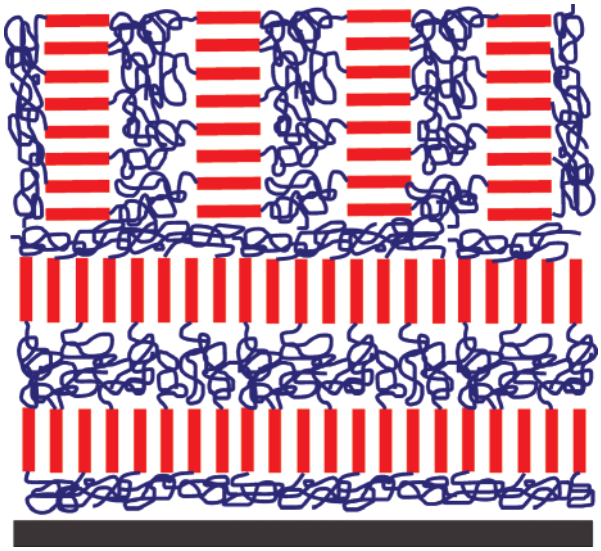

Figure 8. Schematic of smectic A-like lamellar structure in thin films of rod−coil block copolymer. Films of DEH−PPV-*b*-PI rod−coil block copolymers show smectic A-like lamellar structures where the rod normals are oriented parallel to the lamellar normals across a wide range of coil fractions. The bimodal orientation of the lamellae within the film also creates a bimodal orientation of the rod crystallites both parallel and perpendicular to the film surface.

peaks in the first-order Laue zone. In particular, a strong 001 reflection is only observed when the *c*-axis of the PPV unit cell is oriented parallel to the surface normal. Even when this reflection occurs, the axial ordering remains much poorer than the in-plane ordering: while the 110 peak has a full width at half-maximum (fwhm) of 0.25 1/nm (close to the instrumental resolution), the 001 peak has a fwhm of 0.60 1/nm. This templating results from the presence of a sharp interface that serves to enforce a registry on all of the rods, resulting in a highly ordered three-dimensional crystal. The hard interface provided by the film is required, as evidenced by the lack of axial registration in bulk weakly segregated block copolymers where the interface is relatively diffuse.[18]

The 4-fold symmetry of the unit cell suggests that the DEH−PPV molecular conformation and interactions are significantly different from those observed in other alkoxy-PPVs. Previous studies of MEH−PPV and DOO−PPV report that these molecules crystallize in a boardlike arrangement of flat, rigid molecules with extended side chains and strong $\pi-\pi$ interactions.[51,52] The higher symmetry of the DEH−PPV crystal structure implies that the molecules do not assume a flat conformation and that $\pi-\pi$ associations, which would typically result in 2-fold symmetry for in-plane packing, are weak or absent. Relatively weak intermolecular interactions in DEH−PPV are consistent with its lower melting temperature and higher solubility in most solvents.[54] Molecular dynamics simulations of MEH−PPV and DOO−PPV suggest that PPVs may assume nonplanar chain conformations,[63] and dense substitution with achiral and bulky side groups may further disrupt a regular arrangement of chains in a flat and fully extended conformation. On the basis of quantum mechanical energy minimization calculations, the fully extended width of the DEH−PPV repeat unit is 1.982 nm, of the same relative size as the unit cell. While

Table 3. Comparison of Domain Spacing Estimated by ED, GIXD, and WAXS

technique	rod−rod spacing (nm)
GIXD	0.95
ED	1.05
WAXS	0.97

the diffraction information is insufficient to localize the atomic positions in the side chains and the achiral nature of the ethylhexyl groups makes perfectly regular packing impossible, several different packing mechanisms may be envisioned. One plausible structural mechanism is a staggered orientation of the center chain relative to the corner chains so that the side groups of the center chain may pack diagonally across the unit cell. This structure may resemble herringbone packing in unsubstituted PPV[42−45] and would result in large differences in side-chain orientation between the two chains. Axial disorder and twist along the polymer backbone result in differences in the side-chain positions between unit cells, contributing to a relatively disordered crystalline structure.

The thin film structure of DEH−PPV determined by GIXD and ED is in agreement with our previous less detailed WAXS study of bulk DEH−PPV.[54] The thin film GIXD linecut at $q_z = 0.22$ 1/nm shows many of the same peaks as the bulk WAXS profiles, and the rod−rod packing distances (Table 3) are in close agreement. These studies demonstrate square packing in the plane of the rods in both thin films and the bulk, though peak indexing has been refined due to the added information provided by the many higher-order reflections observed in the better ordered thin films.

Analysis of the angular distribution of peak intensities in the GIXD patterns indicates that the 5100 g/mol homopolymers are primarily aligned with the 001 axis perpendicular to the film surface, while in the 3500 g/mol homopolymers the 001 axis is oriented both parallel and perpendicular to the film surface (see Figure 3). In DEH−PPV-5.1, all peaks in the zeroth-order Laue zone are most intense along the $q_z = 0$ axis, indicating that the (110) plane is perpendicular to the sample surface for most of the crystalline regions. However, the intensities of the reflections are arced, indicating that there is a distribution of crystallite orientations. Because of vertical cuts not intersecting the specular axis, the arc intensities are not directly indicative of the orientation distribution. In DEH−PPV-3.5, there is a bimodal distribution, with scattering intensities from the zeroth-order Laue zone concentrated along both the $q_z = 0$ and the vertical cut axes. This suggests that in the 3500 g/mol material the rods become trapped in a mixed orientation with crystallites both perpendicular and parallel to the sample surface. The large intensity of the 110 and 220 reflections along the vertical cut indicates that the molecules in the parallel orientation pack with the 110 axis perpendicular to the substrate. The intensities of the reflections for DEH−PPV-3.5 are much more strongly arced than for DEH−PPV-5.1, indicating that there is significantly more disorder in crystallite orientation for the lower molecular weight sample.

Liquid Crystalline Structure in PPV-*b*-PI Thin Films. The crystalline structure of the DEH−PPV homopolymer persists in rod−coil block copolymers, and this has a large effect on the self-assembled microdomain structures observed in films of these materials below the melting temperature of the DEH−PPV. As described previously, DEH−PPV-*b*-PI diblock copolymers self-assemble into lamellar structures in thin films that demonstrate a mix between lamellae oriented parallel to the surface and lamellae oriented perpendicular to the surface.[36] As thickness is increased, the fraction of perpendicular lamellae at the vacuum interface increases until it is covered by entirely perpendicular lamellae. Figure 6 shows an SFM image of the film studied by GIXD for the polymer with a coil fraction of 0.42. This SFM indicates that for the film thicknesses studied the vacuum interface is dominated by lamellae with a perpendicular nanodomain orientation, and the overall films are composed of a mix of parallel and perpendicularly oriented lamellar nanodomains.

X-ray diffraction allows the crystalline structure and rod orientation within the lamellar nanodomains to be determined. GIXD patterns for four PPV-*b*-PI block copolymers with varying coil fraction (Figure 7) show that the crystal structure of the DEH−PPV is largely preserved in the block copolymers when they are annealed at elevated temperature to induce self-assembly, then cooled, and studied at room temperature (22−23 °C). However, there are subtle changes in the crystal structure with changing coil fraction. The peak positions and indexing in the GIXD for the block copolymers are identical to those for the DEH−PPV homopolymer. The primary difference is that the reflections in the first-order Laue zone become much clearer in the block copolymer; particularly the 101, 111, and 301 reflections become more pronounced. This is due the interplay between microphase separation and smectic alignment and improved alignment in the block copolymer films. After film-casting, the polymers are annealed above the melting temperature to induce microphase separation and then cooled to form crystallites. Microphase separation templates the crystallite growth, resulting in the observation of these higher-order reflections. Increasing coil fraction eventually leads to a strong disruption of the lattice, as shown in Figure 7d for a sample with 82% coil. In this case only the 110 and 220 peaks are visible, and the other reflections are relatively diffuse rings, indicating a relatively large amount of disorder in the rod crystalline lattice. The scattering intensity from the rod lattice is decreased dramatically, and the 220 ring is dwarfed by the amorphous scattering halo from the polyisoprene block.

The three block copolymers with less extreme coil fractions ($\phi_{coil} = 0.42$, 0.67, and 0.72) show peaks corresponding to crystallites oriented with the 001 direction both perpendicular (parallel lamellar microphase) and parallel (perpendicular lamellar microphase) to the film surface. In the 42% PI film, the parallel oriented crystallites show a mixed orientation where a fraction of the crystallites have the 110 vector perpendicular to the interface and a fraction have the 100 vector perpendicular to the interface, as indicated by the intermediate peak in the 110 reflection ring at ∼45°. However, at 67% or 72% coil fraction, all of the crystallites are either oriented with the 001 direction perpendicular to the surface or with the 110 crystallographic direction perpendicular to the surface. At 82% PI the crystal orientation distribution becomes very broad, as indicated by the relatively large angular distribution of the 110 and 220 scattering intensities. As with DEH−PPV homopolymers, surface templating of the block copolymers results in decreased axial disorder and the appearance of a strong 001 reflection only for lamellar layers oriented parallel to the film interface.

GIXD data indicates that the DEH−PPV rods pack parallel to the block copolymer lamellar normal, indicating a smectic A-like lamellar phase for the three block copolymers with the lower coil fractions where the crystalline structure is clearly resolvable. These structures show long-range order typical of self-assembled block copolymers and crystalline DEH−PPV nanodomains, so the nomenclature smectic A-like refers to the orientation of the rod director normal to the lamellar interface, as shown in Figure 8. There is little change in the crystal

structure of the block copolymers with increasing coil fraction. Neither the 110 nor 001 peaks shift in position, indicating that neither the volume nor any of the linear dimensions of the unit cell change with increasing coil fraction. Not only do the DEH−PPV nanodomains exclude the PI block but also the in-plane tensile stress on the DEH−PPV crystallites caused by extension of the PI block causes little distortion of the lattice constants. This indicates that the rod orientation within the unit cell and the number of monomers per unit cell remain constant in a smectic A-like structure to above 72% coil. Several small changes in the relative peak intensities are observed with changing coil fraction. The 220 reflection and other higher-order *hk*0 reflections decrease in intensity relative to the 110 peak with increasing coil fraction, indicating a decrease in the higher-order structure. However, up to 72% coil the fwhm of the 110 peak remains roughly constant at 0.24 1/nm, very close to the instrumental resolution, demonstrating a large crystallite size. When coil fraction is increased to 82%, the 110 fwhm jumps to 0.33 1/nm, consistent with a decrease in crystal size and disordering of the in-plane lattice. The 001 peak also gets progressively less intense relative to the 110 peak, consistent with interfacial broadening and increased axial disorder as the segregation strength is decreased.

In bulk rod−coil block copolymers, it is predicted that an increase in coil fraction should result in a transition from a smectic A-like to a smectic C-like phase due to the increased size of the coil relative to the rod at higher coil fraction.[37−39] Despite the fact that our system is a thin film system, this effect should still occur. Existing predictions of rod tilt in thin films do not explore coil fraction and are restricted to confinement between two hard interfaces, where geometric effects are dominant.[64] The vacuum interface in our thin film system allows most of the material to rearrange to an equilibrium thickness on the basis of the natural domain spacing of the block copolymer, and the preference for the PI block at both interfaces[36] implies that proximity to the interface should not alter the rod tilt angle. However, the smectic A to smectic C transition predicted by scaling theory[37] and self-consistent-field theory[38,39] is not observed in our experimental system. One of the primary differences between the experimental system and the theoretical treatments is that all of the rods in the theoretical treatments show only nematic interactions. Any forces that would lead to smectic structure or crystallization of the rods within the lamellar layers are neglected by the theory as secondary effects. The high degree of crystallinity in these PPV-*b*-PI films suggests that the secondary effects, specific in nature to the individual rod system used in the block copolymer, may be primarily responsible for the absence of an experimentally observed transition between normal rod orientation (smectic A-like) and tilted rod orientation (smectic C-like) within the lamellae. Even for a relatively weakly crystalline system such as DEH−PPV the constraints of packing into the unit cell may dominate over the free energies that lead to transitions in rod tilt.

Conclusions

The crystal structure of DEH−PPV, a soluble and processable photoluminescent polymer, was studied in thin films of homopolymer and rod−coil block copolymer. DEH−PPV packs on a tetragonal lattice with two chains per unit cell. The unit cell dimensions are $a = b = 1.348$ nm and $c = 0.665$ nm, and the unit cell density is 0.95 g/cm^3. The DEH−PPV chain axis aligns parallel to the *c*-axis. The nearest-neighbor spacing between rods is 1.0 nm. In thin films cast from toluene the crystallites align with the chains primarily perpendicular to the surface for molecular weights around 5000 g/mol, but at lower molecular weights (3500 g/mol) the chains have a mixed orientation with some parallel and some perpendicular to the substrate. When chains are oriented parallel to the surface, the 110 crystallographic direction is perpendicular to the interface. For DEH−PPV-*b*-PI rod−coil block copolymers, the crystalline structure of the rod is largely preserved. The block copolymers self-assemble into lamellae in thin films, and the rod packing within the lamellar layers is nearly identical to that of the PPV homopolymer. This gives the lamellae a smectic A-like structure with the rods oriented parallel to the lamellar normal. However, a greater degree of order is observed in the 001 direction due to the effect of microphase separation at registering the chains. The rod tilt relative to the lamellar normal does not change with increasing coil fraction, suggesting that below the melting temperature system specific crystallization effects dominate over chain stretching considerations that would favor an increase in rod tilt with increasing coil fraction. Only minor changes in peak intensities are observed up to a coil fraction of 72%, but further increasing the coil fraction eventually results in a breakdown of most of the crystalline structure between 72% and 82% PI.

Acknowledgment. R.A.S. and B.D.O. gratefully acknowledge support from the ACS-Petroleum Research Fund and an NSF-CAREER Award. E.L.T., D.A., and V.K. acknowledge support from the MIT Center for Materials Science and Engineering (CMSE), supported by the NSF MRSEC program under Award DMR 02-13282. GIXD experiments were performed at the Stanford Synchrotron Radiation Laboratory, a national user facility operated by Stanford University and supported by the Department of Energy, Office of Basic Energy Sciences. This work also made use of shared TEM facilities at the MIT CMSE. B.D.O. gratefully acknowledges the Fannie and John Hertz Foundation for a graduate fellowship.

References and Notes

(1) Friend, R. H.; Gymer, R. W.; Holmes, A. B.; Burroughes, J. H.; Marks, R. N.; Taliani, C.; Bradley, D. D. C.; Dos Santos, D. A.; Bredas, J. L.; Logdlund, M.; Salaneck, W. R. *Nature (London)* **1999**, *397*, 121−128.
(2) Malliaras, G.; Friend, R. *Phys. Today* **2005**, *58*, 53−58.
(3) Heeger, A. J. *Rev. Mod. Phys.* **2001**, *73*, 681−700.
(4) Moons, E. *J. Phys.: Condens. Matter* **2002**, *14*, 12235−12260.
(5) Voigt, M.; Chappell, J.; Rowson, T.; Cadby, A.; Geoghegan, M.; Jones, R. A. L.; Lidzey, D. G. *Org. Electron.* **2005**, *6*, 35−45.
(6) Sivula, K.; Ball, Z. T.; Watanabe, N.; Frechet, J. M. J. *Adv. Mater.* **2006**, *18*, 206−210.
(7) de Boer, B.; Stalmach, U.; van Hutten, P. F.; Melzer, C.; Krasnikov, V. V.; Hadziioannou, G. *Polymer* **2001**, *42*, 9097−9109.
(8) Lin, H. C.; Lee, K. W.; Tsai, C. M.; Wei, K. H. *Macromolecules* **2006**, *39*, 3808−3816.
(9) Hulvat, J. F.; Sofos, M.; Tajima, K.; Stupp, S. I. *J. Am. Chem. Soc.* **2005**, *127*, 366−372.
(10) Yu, W. L.; Meng, H.; Pei, J.; Huang, W.; Li, Y. F.; Heeger, A. J. *Macromolecules* **1998**, *31*, 4838−4844.
(11) Bates, F. S.; Fredrickson, G. H. *Phys. Today* **1999**, *52*, 32−38.
(12) Segalman, R. A. *Mater. Sci. Eng., R* **2005**, *48*, 191−226.
(13) Lee, M.; Cho, B. K.; Zin, W. C. *Chem. Rev.* **2001**, *101*, 3869−3892.
(14) Chen, J. T.; Thomas, E. L.; Ober, C. K.; Mao, G. P. *Science* **1996**, *273*, 343−346.
(15) Radzilowski, L. H.; Carragher, B. O.; Stupp, S. I. *Macromolecules* **1997**, *30*, 2110−2119.
(16) Tenneti, K. K.; Chen, X. F.; Li, C. Y.; Tu, Y. F.; Wan, X. H.; Zhou, Q. F.; Sics, I.; Hsiao, B. S. *J. Am. Chem. Soc.* **2005**, *127*, 15481−15490.
(17) Lee, M.; Cho, B. K.; Kim, H.; Yoon, J. Y.; Zin, W. C. *J. Am. Chem. Soc.* **1998**, *120*, 9168−9179.
(18) Olsen, B. D.; Segalman, R. A. *Macromolecules* **2005**, *38*, 10127−10137.
(19) Olsen, B. D.; Segalman, R. A. *Macromolecules* **2006**, *39*, 7078−7083.

(20) Fasolka, M. J.; Mayes, A. M. *Annu. Rev. Mater. Res.* **2001**, *31*, 323−355.
(21) Harrison, C.; Dagata, J. A.; Adamson, D. H. In *Developments in Block Copolymer Science and Technology*; Hamley, I. W., Ed.; John Wiley & Sons: New York, 2004; pp 295−323.
(22) Leclere, P.; Calderone, A.; Marsitzky, D.; Francke, V.; Geerts, Y.; Mullen, K.; Bredas, J. L.; Lazzaroni, R. *Adv. Mater.* **2000**, *12*, 1042−1046.
(23) Wang, H. B.; Wang, H. H.; Urban, V. S.; Littrell, K. C.; Thiyagarajan, P.; Yu, L. P. *J. Am. Chem. Soc.* **2000**, *122*, 6855−6861.
(24) Leclere, P.; Hennebicq, E.; Calderone, A.; Brocorens, P.; Grimsdale, A. C.; Mullen, K.; Bredas, J. L.; Lazzaroni, R. *Prog. Polym. Sci.* **2003**, *28*, 55−81.
(25) Hempenius, M. A.; Langeveld-Voss, B. M. W.; van Haare, J.; Janssen, R. A. J.; Sheiko, S. S.; Spatz, J. P.; Moller, M.; Meijer, E. W. *J. Am. Chem. Soc.* **1998**, *120*, 2798−2804.
(26) Stupp, S. I.; LeBonheur, V.; Walker, K.; Li, L. S.; Huggins, K. E.; Keser, M.; Amstutz, A. *Science* **1997**, *276*, 384−389.
(27) Surin, M.; Marsitzky, D.; Grimsdale, A. C.; Mullen, K.; Lazzaroni, R.; Leclere, P. *Adv. Funct. Mater.* **2004**, *14*, 708−715.
(28) Park, J. W.; Thomas, E. L. *Adv. Mater.* **2003**, *15*, 585−588.
(29) Park, J. W.; Thomas, E. L. *Macromolecules* **2006**, *39*, 4650−4653.
(30) Minich, E. A.; Nowak, A. P.; Deming, T. J.; Pochan, D. J. *Polymer* **2004**, *45*, 1951−1957.
(31) Liu, J. S.; Sheina, E.; Kowalewski, T.; McCullough, R. D. *Angew. Chem., Int. Ed.* **2001**, *41*, 329−332.
(32) Yang, X.; Loos, J. *Macromolecules* **2007**, *40*, 1353−1362.
(33) Guarini, K. W.; Black, C. T.; Yeuing, S. H. I. *Adv. Mater.* **2002**, *14*, 1290−1294.
(34) Heiser, T.; Adamopoulos, G.; Brinkmann, M.; Giovanella, U.; Ould-Saad, S.; Brochon, C.; van de Wetering, K.; Hadziioannou, G. *Thin Solid Films* **2006**, *511*, 219−223.
(35) Leclere, P.; Parente, V.; Bredas, J. L.; Francois, B.; Lazzaroni, R. *Chem. Mater.* **1998**, *10*, 4010−4014.
(36) Olsen, B. D.; Segalman, R. A. *Macromolecules*, in press.
(37) Semenov, A. N. *Mol. Cryst. Liq. Cryst.* **1991**, *209*, 191−199.
(38) Pryamitsyn, V.; Ganesan, V. *J. Chem. Phys.* **2004**, *120*, 5824−5838.
(39) Matsen, M. W.; Barrett, C. *J. Chem. Phys.* **1998**, *109*, 4108−4118.
(40) Kinder, L.; Kanicki, J.; Petroff, P. *Synth. Met.* **2004**, *146*, 181−185.
(41) Pattison, L. R.; Hexemer, A.; Kramer, E. J.; Krishnan, S.; Petroff, P. M.; Fischer, D. A. *Macromolecules* **2006**, *39*, 2225−2231.
(42) Granier, T.; Thomas, E. L.; Gagnon, D. R.; Karasz, F. E.; Lenz, R. W. *J. Polym. Sci., Part B: Polym. Phys.* **1986**, *24*, 2793−2804.
(43) Chen, D.; Winokur, M. J.; Masse, M. A.; Karasz, F. E. *Polymer* **1992**, *33*, 3116−3122.
(44) Mao, G.; Fischer, J. E.; Karasz, F. E.; Winokur, M. J. *J. Chem. Phys.* **1993**, *98*, 712−716.
(45) Bradley, D. D. C. *J. Phys. D: Appl. Phys.* **1987**, *20*, 1389−1410.
(46) Capaz, R. B.; Caldas, M. J. *Phys. Rev. B* **2003**, *67*, 205205.
(47) Zheng, G.; Clark, S. J.; Brand, S.; Abram, R. A. *J. Phys.: Condens. Matter* **2004**, *16*, 8609−8620.
(48) Resel, R.; Kiebooms, R.; Vanderzande, D.; Stelzer, F. *Monatsh. Chem.* **2001**, *132*, 433−440.
(49) Martens, J. H. F.; Marseglia, E. A.; Bradley, D. D. C.; Friend, R. H.; Burn, P. L.; Holmes, A. B. *Synth. Met.* **1993**, *55*, 449−453.
(50) Gill, R. E.; Meetsma, A.; Hadziioannou, G. *Adv. Mater.* **1996**, *8*, 212−214.
(51) Chen, S. H.; Su, A. C.; Chou, H. L.; Peng, K. Y.; Chen, S. A. *Macromolecules* **2004**, *37*, 167−173.
(52) Chen, S. H.; Su, A. C.; Han, S. R.; Chen, S. A.; Lee, Y. Z. *Macromolecules* **2004**, *37*, 181−186.
(53) Babudri, F.; Cicco, S. R.; Farinola, G. M.; Naso, F.; Bolognesi, A.; Porzio, W. *Macromol. Rapid Commun.* **1996**, *17*, 905−911.
(54) Olsen, B. D.; Jang, S. Y.; Luning, J. M.; Segalman, R. A. *Macromolecules* **2006**, *39*, 4469−4479.
(55) Jeng, U.; Hsu, C. H.; Sheu, H. S.; Lee, H. Y.; Inigo, A. R.; Chiu, H. C.; Fann, W. S.; Chen, S. H.; Su, A. C.; Lin, T. L.; Peng, K. Y.; Chen, S. A. *Macromolecules* **2005**, *38*, 6566−6574.
(56) Yang, C. Y.; Hide, F.; Diaz-Garcia, M. A.; Heeger, A. J.; Cao, Y. *Polymer* **1998**, *39*, 2299−2304.
(57) Resel, R.; Tertinek, B.; Tasch, S.; Davey, A.; Blau, W.; Horhold, H. H.; Rost, H.; Leising, G. *Synth. Met.* **1999**, *101*, 96−97.
(58) Olsen, B. D.; Segalman, R. A. *Macromolecules*, in press.
(59) Chabinyc, M. L.; Toney, M. F.; Kline, R. J.; McCulloch, I.; Heeney, M. *J. Am. Chem. Soc.* **2007**, *129*, 3226−3237.
(60) Minter, J. R.; Shimamura, K.; Thomas, E. L. *J. Mater. Sci.* **1981**, *16*, 3303−3308.
(61) Shimamura, K.; Minter, J. R.; Thomas, E. L. *J. Mater. Sci. Lett.* **1983**, *2*, 54−58.
(62) Suehiro, K.; Chatani, Y.; Tadokoro, H. *Polym. J.* **1975**, *7*, 352−358.
(63) Yang, H. C.; Hua, C. Y.; Kuo, M. Y.; Huang, Q.; Chen, C. L. *ChemPhysChem* **2004**, *5*, 373−381.
(64) Pereira, G. G.; Williams, D. R. M. *Macromolecules* **2000**, *33*, 3166−3172.

MA0714971